Available online at www.sciencedirect.com
ScienceDirect
Proceedings of the Combustion Institute 32 (2009) 2231–2238
Proceedings of the Combustion Institute
www.elsevier.com/locate/proci

Nonane droplet combustion with and without buoyant convection: Flame structure, burning rate and extinction in air and helium

J.H. Bae [1], C.T. Avedisian *

Sibley School of Mechanical and Aerospace Engineering, Cornell University, Ithaca, NY 14853-7501, USA

Abstract

The burning and extinction characteristics of isolated small nonane droplets are examined in a buoyant convective environment and in an environment with no external axial convection (as created by doing experiments at low gravity) to promote spherical droplet flames. The ambience is air and a mixture of 30%O_2/70%He to assess the influence of soot formation. The initial droplet diameter (D_o) ranges from 0.4 to 0.95 mm. Measurements are reported of the extinction diameter and time to extinction, and of the evolution of droplet diameter, flame diameter, soot shell diameter, burning rate, and broadband radiative emissions.

In a buoyancy-free environment for air larger droplets burn slower than smaller droplets for the range of D_o examined, which is attributed to the influence of soot. In the presence of a buoyant flow in air, no influence of D_o is observed on the burning rate while the buoyant flames are still heavily sooting. The effect of D_o is believed to be due to a combination of dominance of the nonluminous, nonsooting, portion of the buoyant flame around the forward half of the droplet on heat transport and the secondary role of the luminous wake portion of the flame. In a non-sooting helium inert at low gravity, no effect of D_o is found on the evolution of droplet diameter.

Flame extinction is observed only in the 30%O_2/70%He ambience. For all of the observations, extinction appears to occur before the disappearance of the droplet which is then followed by a period of evaporation. The extinction diameter and time to extinction increases with D_o and an empirical correlation is presented for these two variables.

Keywords: Droplet; Soot formation; Microgravity; Spray; Surrogate

1. Introduction

This paper examines the combustion process of an isolated *n*-nonane droplet (C_9H_{20}, $T_b = 424$ K, $T_c = 595$ K, $P_c = 2.3$ MPa [1]) in an ambience that can promote or suppress soot formation and flame extinction, and under conditions where the droplet flame is spherical or strongly influenced by buoyant convection. *n*-nonane is strongly sooting in air which allows examination of the influence of sooting, previous experience exists with nonane which facilitates experimentation [2,3], and it is a surrogate constituent for a model transportation fuel [4]. The case of spherical gas phase symmetry is realized

* Corresponding author. Fax: +1 607 255 1222.
E-mail address: cta2@cornell.edu (C.T. Avedisian).
[1] Present address: Sensata Technologies, 529 Pleasant Street, Attleboro, MA 02702, USA.

1540-7489/$ - see front matter © 2009 Published by Elsevier Inc. on behalf of The Combustion Institute.
doi:10.1016/j.proci.2008.06.221

by a combination of restricting the droplet's ability to move during burning and by carrying out the experiments in a gravitational field that is low enough so that the effect of buoyancy is considerably reduced. A motivation of the study is to produce data that can be used as a basis for validating detailed numerical models of the droplet burning process, refining such models, and extending them to include new phenomenon (e.g., soot). Spherical droplet flames are ideal for modeling and data for this configuration are now being used for validation [5–8].

The present study builds on previous work which examined the influence of liquid and gas phase composition on spherically symmetric nonane droplet combustion which showed that at the highest inert dilution by helium examined (i.e., a gas comprised of 30%O_2/17% N_2/53%He, volume percent), flame extinction did not occur. In the present study the inert is increased to 100% helium (a composition of 30%O_2/70%He) and flame extinction is now observed. Data are reported on the extinction diameter (D_e), time to extinction (t_e), and evolution of flame diameter, droplet diameter, soot shell diameter, and broadband radiative emissions that is indicative of soot formation.

2. Experimental

The general procedures for the low gravity experiments are similar to those described previously [2,3,9,10]. To promote spherical gas phase symmetry, the experimental package containing the test droplet is released into free-fall to create a low buoyancy environment and the experiments are conducted during the fall. For buoyant droplet flames, the same package is used except that the package is not dropped. The test droplets are contained in a sealed chamber which is filled with the gas mixture of interest, which here is room temperature air or a gas composition of 30%O_2/70%He. These two gases produce large differences in sooting trends. The initial droplet diameters examined, D_o, are between 0.4 and 0.95 mm. The chamber volume measuring 19 cm × 18 cm × 25 cm was sufficiently large ($\sim 10^{-5}$ m^3) compared to the droplet volume ($\lesssim 10^{-9}$ m^3) or resulting vapor volume ($\sim 10^{-7}$ m^3) after droplet evaporation that droplet burning would have little influence on ambient gas volume fraction.

The influence of buoyancy on burning in the laboratory ($g \sim 9.8$ m/s^2) and free fall ($g \sim 0.001$ m/s^2) reference frames is anticipated based on a correction for the spherically symmetric burning rate [11], which can be put in the form $K/K_o \sim 1 + f$ where $f \approx aRa^b$, Ra is the Rayleigh number when the Prandtl number is close to unity, $a \approx 0.533$, $b \approx 0.52$ and $K_o \equiv |\frac{dD^2}{dt}|$ which itself could be dependent on D_o [12–15]. Considering first normal gravity, evaluating gas properties [16] at 1200 K, assuming that properties are bounded by air, helium, CO_2 or H_2O and taking $0.4\text{ mm} < D_o < 0.95\text{ mm}$, shows that $0.01 < f_{He} < 0.05$, $0.002 < f_{CO_2} < 0.008$, $0.07 < f_{air} < 0.3$ and $0.12 < f_{H_2O} < 0.5$. Convection could then exert some influence on burning rate depending on the gas composition. For $g \sim 0.001$ m/s^2 and using properties of any of these gases shows that $f \ll 1$ for even the largest D_o considered. The ambient gas mixture (air or 30%O_2/70%He) is stored in pre-prepared bottles and introduced into the chamber under vacuum until the pressure is increased to atmospheric.

Droplets are anchored by two SiC fibers (diameter, $D_{fiber} = 12$ μm) crossed at an angle of about 60° and mounted on support stands. Previous work showed that this fiber support configuration did not appreciably influence the evolution of droplet diameter when compared with free-floating droplets for the majority of the burning period [17,18]. As with all fiber support techniques, however, the fiber will influence droplet burning when $D_{fiber} \sim D$. The fiber can serve as a conduction path for heat transfer to the droplet or as an attactor of soot aggregates. Precisely how small a droplet must be for heat transfer through the fiber to be appreciable requires comparing conduction through the fiber to radiative and conductive transport from the flame to the droplet through the gas. Conduction through the fiber is estimated by assuming the sides of the fiber are insulated, and with one end of the fiber at the flame temperature (taken as 1500 K) and the other at the droplet temperature (424 K). With the droplet and flame being concentric spheres at different temperatures, and taking $D_f/D \sim 10$ (an average value), we find for a fiber thermal conductivity of 60 W/mK that roughly 10% of the heat to the droplet comes through the fiber when $D \sim 200$ μm which is the smallest extinction diameter measured in the present experiments. The remaining 90% of the heat comes from radiation and gaseous conduction. The fiber influence associated with sooting dynamics [19] appeared to be minimal for the present conditions.

The test droplet is ignited by heating two Kanthal A-1 (33 AWG) wires positioned on opposite sides of the droplet to reduce ignition asymmetries. The wires are formed into 0.5 mm ID loops by wrapping them around a #76 drill. They are positioned from 0.50 to 1 mm from the droplet surface and attached to solenoid values through ceramic rods to retract the wires after ignition. The droplet burning process is recorded by two cameras, one for observing the droplet and soot structure (16-mm LOCAM II camera with black and white film) and the other for recording flame images (Hitachi HV-C20 CCD video camera). Individual film frames are analyzed by Image

Pro-Plus 4.0 on a PC. The smallest diameter that could be resolved with the lenses and optics uses is about 40 μm [9].

Sooting tendencies are assessed for the low gravity flames (only) by measuring the broadband emission produced during the droplet burning process [10,18]. The concept is less quantitative than soot volume fraction measurements [13] but still useful and relatively easy to implement in a microgravity platform. The amplified output voltage from the photodiode is collected with a Labview program through a cable to the drop-package. We used the photodiode voltage as a measure of sooting trends to the extent it is reasonable to do so consistent with the literature on using a photodiode to probe sooting droplet flames (as discussed in [20]). Broadband emission is indicative of soot formation if the droplet flame temperature does not change with parameters for a given gas composition and if soot aggregates do not pass through the flame where they would be oxidized and contribute to emissions (this is not the case for buoyant flames where aggregates are forced through the wake of the flame and oxidize). For spherical flames that essentially enclose aggregates, the flame luminosity would be attributed to incandescence. The intersection of the fiber and flame produces a 'glow' that could also influence the radiation field.

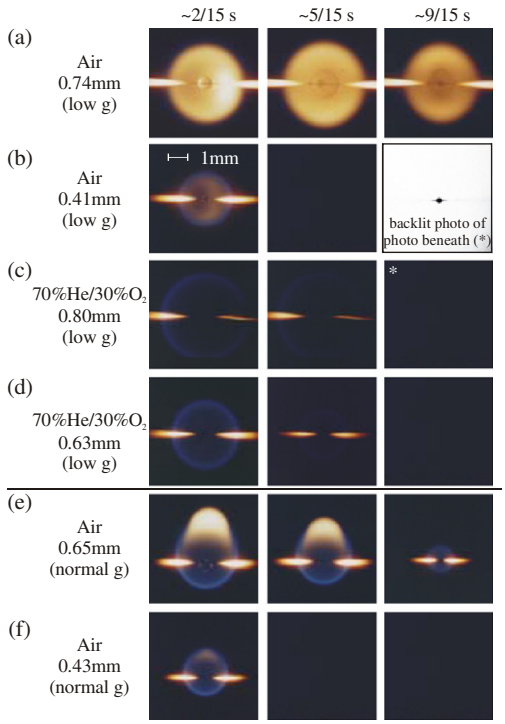

Fig. 1. Selected color images showing flame structure for spherical flames (a–d) and buoyant wake-like droplet flames (e and f). Initial droplet diameter is indicated adjacent to each row. Time after ignition is given at the top of each column. (For interpretation of the references to color in this figure legend, the reader is referred to the web version of this paper.)

3. Results and discussion

3.1. Droplet flame images

Figure 1 shows representative photographs from the movie record of flame-illuminated images of nonane droplets for the indicated D_o. Figure 1a and b shows spherical flames for burning in air at low gravity[2] for two different initial diameters, and Fig. 1c and d shows representative droplets in 30%O_2/70%He also in low gravity. The droplet is somewhat visible through the flame in Fig. 1a and development of the soot shell is evident. The flame structure of the smaller droplet (Fig. 1b) exhibits the characteristic outer blue zone indicative of CH emissions and an inner core associated with soot incandescence.

The large droplet of Fig. 1a shows a significantly more luminous flame in air than the smaller droplet of Fig. 1b which indicates more soot than smaller droplets. The reason for D_o's influence on sooting trends was previously discussed in terms of comparing the residence time of fuel molecules with a pyrolysis chemical time as [21] $D_c = A\frac{D_o^2}{\alpha}\exp\left(\frac{-E}{RT}\right)$ where E is an activation energy associated with a first-order pyrolysis reaction, A (s^{-1}) is the corresponding pre-exponential factor and α is the gas thermal diffusivity. Increasing D_o raises D_c and the propensity for sooting which is qualitatively consistent with Fig. 1a and b.

When the inert is replaced by helium, the yellow luminosity indicative of soot incandescence is virtually eliminated for a given D_o (compare Fig. 1a with Fig. 1c and d). This effect is a consequence of helium's influence on flame temperature such that the flame is apparently not hot enough to reach the soot inception temperature [22].

Flame extinction was observed as the physical disappearance of the flame. Figure 1c illustrates this at 9/15 s after ignition. This photograph is representative of the difficulty to observe disappearance of the flame, which complicates detecting extinction. The black and while photograph shown in Fig. 1b is a companion to the last color[3] photograph in Fig. 1c which shows the drop without a visible flame.

[2] The black and white photograph in the third column of Fig. 1b belongs at the end of the third column of Fig. 1c but is included in the second row for compactness.

[3] For interpretation of the references to color in Fig. 1, the reader is referred to the web version of this paper.

For burning in air at the Earth's normal gravity (Figs. 1e and f), the buoyant flow shows a typical hybrid structure of a blue zone in the forward hemisphere of the droplet and a luminous wake zone. Buoyant convection transports fuel molecules from the upstream portion of the flame into the wake where they pyrolize and undergo the processes which lead to formation of soot [22], and through the flame where they oxidize and produce a yellow wake shown in Figs. 1e and f. Reducing D_o for these convective flames makes them more spherical even at normal gravity, an effect traced to the reduction of Rayleigh number (since $Ra \sim D^3$). Furthermore, the flame is less luminous as D_o decreases (cf Figs. 1e and f) due to a combination of reduced convection as D_o decreases and reduced soot formation (the aforementioned residence time effect).

The soot shell is clearly shown in the collection of backlighted images of Fig. 2 for burning in air for $D_o = 0.73$ mm (Fig. 2a), 0.57 mm (Fig. 2b) and 0.45 mm (Fig. 2c). The photographs were selected at the same fractional period of the burning process (i.e., at the same value of t/t_b where t_b is the burning time defined as the time when the flame was no longer visible) for comparison. The sooting dynamics are similar to previous observations for nonane and heptane droplets [3,14,23,24]. For burning in 30%O_2/70%He no soot was visible in the backlighted images (compare color photographs are shown in Fig. 1c and d). Backlighted images of non-sooting droplets showed only a droplet in a bright background with no soot present.

Early on where the aggregates are very small, they are well positioned between the droplet and flame (Fig. 2a, at $t/t_b \sim 0.3$) and do not drift from the position where forces on them balance. As the aggregates grow they begin to drift as shown in Fig. 2a (0.6) because the forces pushing them back to the equilibrium position are reduced resulting in unstable shells over time. Also, as shown in Fig. 2 the shell 'density' is reduced as D_o decreases (compare any column at the same t/t_b), which further shows qualitative evidence for D_o's effect on reducing soot.

The evolution of broadband intensity is shown in Fig. 3 for burning in air at low gravity. In the 30%O_2/70%He ambience the emission was below detectable levels. The intensity profile for $D_o = 0.73$ mm is for the same drop as shown in Fig. 1a. The arrows indicate intensities corresponding to the three images of Fig. 1a. The intensities rise rapidly as soot forms and reach a peak between 15% and 25% of the burning period. They then decrease as the flame becomes physically smaller and abruptly drops to below detectable levels at burnout. As D_o decreases the intensity profiles fall which suggests less soot formation. This trend is also consistent with quantitative soot

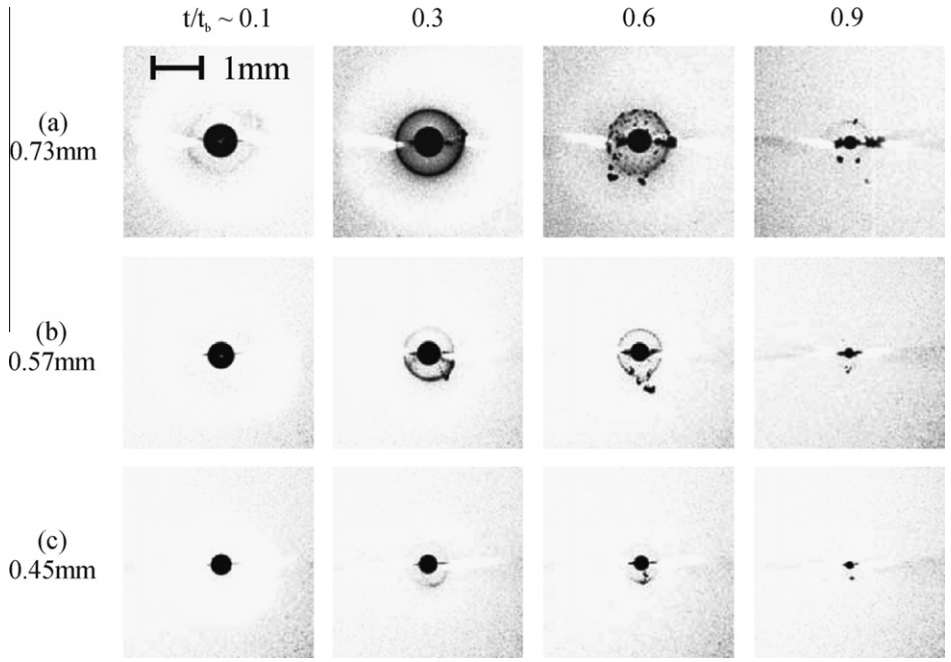

Fig. 2. Selected backlighted images showing development of a soot shell for burning in air at low gravity. Initial droplet diameter is shown adjacent to each row and relative burning time is indicated at the top of each column. Note that for nonsooting conditions, very similar images are found but with no visible black ring.

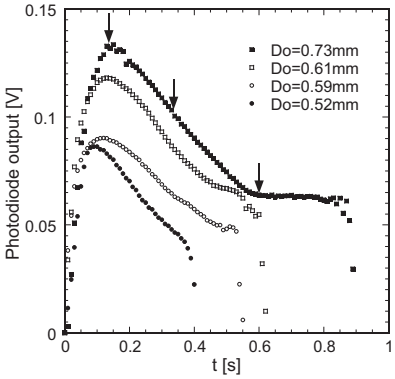

Fig. 3. Evolution of photodiode output for indicated initial droplet diameters showing rise due to soot incandescence and decay as flame burns out. The arrows correspond to the three photographs of Fig. 1a.

volume fraction measurements of spherical heptane droplet flames [13]. It should be noted that only relative sooting trends can be inferred from photodiode output, which nonetheless is still more quantitative than comparing photographic image intensity such as in Fig. 2.

3.2. Quantitative measurements

The evolution of drop D^2 is shown for burning in air at low gravity (Fig. 4a) and in 30%O_2/70%He ambience at low gravity (Fig. 4b) using scaling of variables suggested by the classical theory of droplet burning [25]: $(D/D_o)^2$ vs t/D_o^2. The data for $D_o = 0.86$ mm in Fig. 4a are limited because residual soot, formed early in the process, obscured the droplet image late in the burning process for the $D_o = 0.86$ mm droplet so that D could not be accurately measured. Also shown in Fig. 4a and b are burning rates obtained by fourth-order polynominal fits. The fourth-order polynomial is selected only to illustrate trends (high order fits can produce nonphysical trends) and to facilitate discussion of the influence of parameters on burning rate.

In air, the burning rate increases throughout as shown in Fig. 4a which runs counter to the classical theory [25]. The increase in the burning may be attributed to droplet heating or fuel vapor accumulation effects [26–28]. In 30%O_2/70%He (Fig. 4b) the burning rate first increases then, about midpoint into the burning process, it decreases. We attribute this initial increase to droplet heating, and the reduction later in the burning process to the approach to an extinction condition (disappearance of the flame) which is manifested by a "tail" at the end of burning as shown in Fig. 4b. Quasi-steady conditions as characterized by a period of relative constancy of the burning rate are clearly not achieved as shown in Fig. 4a and b.

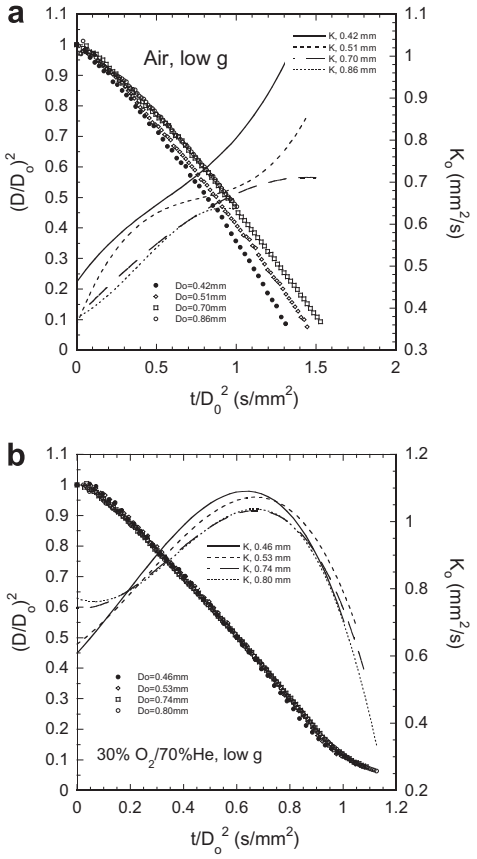

Fig. 4. (a) Evolution of droplet diameter and burning rate (K_o) in air under low gravity (spherical droplet flames (e.g., Fig. 1a and b)) for indicated initial droplet diameters. (b) Evolution of droplet diameter and burning rate (K_o) for burning in 30%O_2/70%He under low gravity (spherical droplet flames (e.g., Fig. 1c and d)) for indicated initial droplet diameters.

Comparing K_o values at any given time shows that in air at low gravity (Fig. 1a) K_o increases with decreasing D_o as shown in Fig. 4a. For burning in 30%O_2/70%He (Fig. 4b) where soot formation is eliminated (flame structure is shown in Figs. 1c and d) variations of D_o exert much less of an effect on K_o and the burning rates are all but independent of D_o (Fig. 4b). Considering that differentiation amplifies uncertainty, the closeness of the $K_o(t)$ variations in Fig. 4b suggests that for the nonsooting flame K_o is essentially independent of D_o.

Under the action of a strong buoyant convective flow (Fig. 5), the larger droplets examined show some evidence for quasi-steady burning over the range $0.5 < t/D_o^2 < 1$ within which the burning rate is somewhat constant. At normal gravity (Figs. 1e and f) the evolutions of (D/D_o^2) with t/D_o^2 show that the smallest drop ($D_o = 0.42$ mm) burns at a slightly higher rate than the largest drop ($D_o = 0.95$ mm) for the latter half of the burning

process. This trend is distinctly different than for burning in air but without any externally driven convection (compare solid circle data between Figs. 4a and 5). As discussed in Section 2, $K/K_o(D_o) \sim 1 + f$ where a functional dependence of K_o on D_o also arises (e.g., Fig. 4a). Since $f \sim D^{3b}$ while K_o decreases with increasing D_o (Fig. 4a), the effects of droplet diameter are competing between the buoyant and nonbuoyant flames: increasing D_o lowers K_o for a sooting spherical droplet flame (due to the thermal effect of soot which arises from a combination of radiative losses and chemical heat effects); increasing D_o in the presence of convection should raise K based on the convective correction to the burning rate. Figure 5 shows that the increase of K brought about by raising initial droplet diameter is apparently enough to nearly collapse the measurements as convection all but eliminates an influence of D_o on burning, when compared with comparable ambient conditions (Fig. 4a) but with no convection.

Convection's influence on the flame structure may also play a role in the complex interplay between burning rate and droplet diameter. We know that blue (nonsooting) spherical droplet flames (Fig. 1c) produce a weak or no dependence of K_o on D_o (Fig. 4b). Convection may create a flame structure even for a sooting fuel that exposes the droplet to the blue nonsooting forward portion of the flame (Fig. 1e) which could dominate heat transport, and with effects of sooting swept through the wake and away form the droplet thus creating a burning process like that of a non-sooting flame. This picture is somewhat consistent with Fig. 5.

Previous work has applied a more generalized empirical scaling for a 30%O_2 ambience as [3] $\left(\frac{D}{D_o}\right)^{2(1+\varepsilon)} = 1 - K'_o(\phi)\frac{t}{D_o^{2(1+\varepsilon)}}$ where ε is a correction

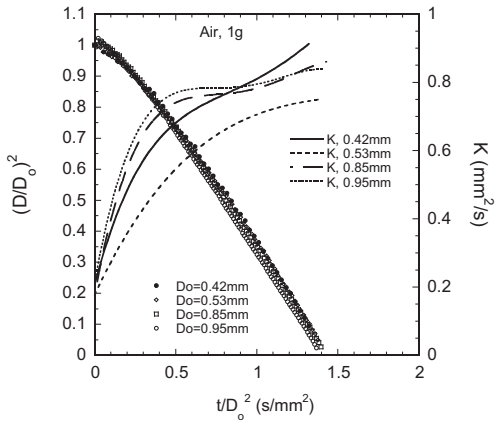

Fig. 5. Evolution of droplet diameter and burning rate (K) in air under normal gravity (buoyant droplet flames (e.g., Fig. 1e and f)).

to the classical result $\varepsilon = 0$, and ϕ is the volume fraction of nitrogen in the remaining 70% inert of a 30%O_2/70% inert ambient gas. Both ε and K' were previously shown to be functions of ϕ. For a pure helium inert, we find from the present results that $\varepsilon \approx 0.025$ best represents the measurements for D_o ranging from 0.45 to 0.9 mm (i.e., for $\phi = 0$, instead of a D^2 law we would have a $D^{2.05}$ law). This value is the same as reported previously from the correlation $\varepsilon = 0.024886 + 0.3104\phi - 0.2457\phi^2 + 0.0533\phi^3$ [3]. We also found that $K'_o \approx 0.9361\ \text{mm}^{2.05}/\text{s}$ (which differs slightly from the value $0.9574\ \text{mm}^{2.05}/\text{s}$ reported previously, though the difference is not great). Comparing Fig. 4a and b for spherical droplet flames suggests that soot formation is responsible for the influence of D_o on the burning rate in air (Figs. 1a and 4a) because without soot (Figs. 1c and 4b) the variation is all but eliminated.

Extinction was revealed by both disappearance of the visible chemiluminescence and the appearance of a 'tail' in the evolution of D^2 (see Fig. 4b). It only occurred for burning in the 30%O_2/70%He ambience. When extinction occurred the flame generally disappeared before the droplet (consistent with quasi-steady predictions [28] even though the present data are not quasi-steady) though flame visibility is poor for the blue nonsooting flames (Figs. 1c and d) near the end of burning. This fact adds considerable uncertainty to identifying the droplet diameter at extinction (D_e) and the time at which the flame extinguishes, t_e. Nonetheless, we show the variation D_e and t_e with D_o from our measurements in Fig. 6. An ad hoc correlation is $D_e \approx 0.337 D_o^{0.56}$ and $t_e \approx 1.01 D_o^{2.218}$ with the lines in Fig. 6 showing these correlations along with uncertainty bars on the measurements. The units for D_e, D_o and t_e are millimeters and seconds, respectively, and the gas composition is 30%O_2/70%He.

Previous modeling efforts have predicted how D_e depends on D_o from the standpoint of nonluminous radiation and conduction loss mechanisms [23], and fuel leakage and finite rate kinetic effects [28,29] assuming quasi-steady conditions (though our data are not quasi-steady). It was shown [7] that including nonluminous radiation in a model of heptane droplet combustion leads to extinction; when it is neglected droplets burn to completion. For the small droplet sizes relevant to the present study, nonluminous radiation is probably negligible [30]. This leaves conductive and luminous radiative loss mechanisms, and fuel leakage effects as possible mechanisms. We are unable to quantitatively determine the effect of luminous radiative losses on extinction since a model of droplet burning has not yet been developed which includes soot formation, complex chemistry and radiation [31]. As noted previ-

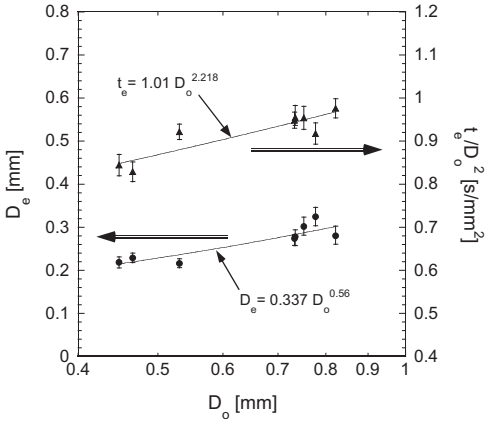

Fig. 6. Variation of extinction diameter (D_e) and extinction time (t_e) with D_o.

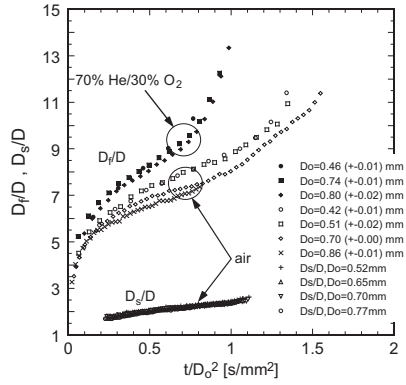

Fig. 7. Evolution of flame and soot shell standoff ratio under low gravity (spherical droplet flames (e.g., Fig. 1a–d)). Ambience is air and 30%O_2/70%He.

ously radiation can influence the propensity for extinction. However, a purely radiative extinction process [29] is unlikely for the comparatively small droplet sizes of interest in the present study.

Numerical analyses predict the importance of conduction loss mechanisms for methanol droplet combustion [5–7,32] and experiments for heptane flame extinction suggest it as well [23]. The high relative thermal conductivity of helium makes conductive losses a viable contributor to extinction. As D_o increases, the flame size increases as well which in turn increases conduction to the surroundings.

Analysis of fuel leakage leads to a critical Damkohler number below which the flame cannot be sustained. For a fixed pressure, it was shown that [28] $K_o D_e \sim$ constant. Accepting that K_o decreases with increasing D_o, if only slightly in the helium inert (Fig. 4b), and further that the simplest relationship would be $K_o \sim 1/D_o$, then $D_e \sim D_o$ which is qualitatively consistent with the observed trends (Fig. 6). The role of internal liquid motion on extinction also deserves mention as apparently only when liquid motion is considered (e.g., induced by motion of the method of droplet deployment, or surface tension gradients inside the droplet) do predicted extinction diameters agree with measurements [5–7].

Figure 7 shows selected data for the evolution of flame and soot shell standoff ratios, D_f/D and D_s/D, for different D_o for the same droplets as in Fig. 4a and b. Only spherical flame (low gravity) data are shown. D_s/D is situated between the droplet and flame as expected because of the forces acting on soot aggregates [33]. It increases only slightly though it roughly tracks with D_f/D.

In the 30%O_2/70%He ambience, as D_o increases D_f/D decreases only slightly at a given scaled time (Fig. 7). With increasing D_o the flame size physically increases which increases diffusive (i.e., conductive) heat losses. The flame would then move closer to the droplet to compensate. Comparing the flame standoff ratio between air (open symbols) and 30%O_2/70%He (closed symbols) shows that the standoff ratio is lower in air than in 30%O_2/70%He. Simple stoichiometry considerations will pull the flame close to the droplet when the oxidizer concentration is increased, even without soot formation. The greater effect of D_o in air than in 30%O_2/70%He on D_f/D may be due to soot formation with its associated luminous radiative effects in addition to diffusive losses, since increasing D_o also increases soot formation.

4. Summary

1. The effect of initial droplet diameter on burning rate is suppressed for a buoyant droplet flame, due to a combination of the complex relationship between burning rate on D_o and flame structure.
2. Without axial convection, larger droplets burning in air where soot formation occurs burn slower than smaller droplets for the range of D_o examined. The effect is attributed to the influence of soot. On the other hand, when soot formation is eliminated as for burning in 30%O_2/70%He, no effect of D_o is found.
3. Flame extinction is observed for the spherically symmetric flame only in the 30%O_2/70%He ambience and not in air. It typically occurred before the completion of burning which was then followed by a period of evaporation.
4. The extinction diameter and time to extinction increases with D_o and an empirical correlation is presented for these two variables. The mechanism for extinction is conjectured to be conductive heat loss from the flame or fuel leakage rather than radiative effects because luminous radiation does not occur in the

30%O_2/70%He environment and the droplet sizes investigated are probably too small for nonluminous radiation to be a factor.

5. Burning was unsteady over the droplet lifetime which is attributed to droplet heating that persists throughout burning or fuel vapor accumulation effects.
6. The spherically symmetric flame standoff ratio is more strongly influenced by D_o in air than in 30%O_2/70%He where there is no soot formation. Soot formation (in air) increases luminous radiative losses as D_o increases which situates the flame closer to the droplet compared to burning in 30%O_2/70%He.

Acknowledgments

The authors are pleased to acknowledge the support of the National Aeronautics and Space Administration (Grant No. NNX08A151G) with Dr. Merril King as Program Director and Michael Hicks as project monitor. The authors also wish to thank Daniel Dietrich of NASA for his interest in our work.

References

[1] D.R. Lide, *Basic Laboratory and Industrial Chemicals*, CRC Press, Boca Raton, FL, 1993, p. 229.
[2] C.T. Avedisian, B.J. Callahan, *Proc. Combust. Inst.* 28 (2000) 991–997.
[3] J.H. Bae, C.T. Avedisian, *Proc. Combust. Inst.* 31 (2007) 2157–2164.
[4] W. Tsang, *Workshop on Combustion Simulation Databases for Real Transportation Fuels*, Report No. NIST-IR-7155, National Institute of Standards and Technology, Gaithersburg, MD, 2003.
[5] V. Raghavan, D.N. Pope, D. Howard, G. Gogos, *Combust. Flame* 145 (2006) 791–807.
[6] B.L. Zhang, J.M. Card, F.A. Williams, *Combust. Flame* 105 (1996) 267–290.
[7] A.J. Marchese, F.L. Dryer, V. Nayagam, *Combust. Flame* 116 (1999) 432–459.
[8] D.L. Dietrich, P.M. Struk, M. Ikegami, G. Xu, *Combust. Theory Model.* 9 (2005) 569–585.
[9] J.H. Bae, Ph.D. Thesis, Sibley School of Mechanical and Aerospace Engineering, Cornell University, 2005.
[10] J.H. Bae, C.T. Avedisian, *Combust. Flame* 145 (2006) 607–620.
[11] C.K. Law, F.A. Williams, *Combust. Flame* (1972) 393–405.
[12] G. Xu, M. Ikegami, S. Honma, et al., *Int. J. Heat Mass Transfer* 46 (2003) 1155–1169.
[13] O.L. Lee, S.L. Manzello, M.Y. Choi, *Combust. Sci. Technol.* 132 (1998) 139–156.
[14] G.S. Jackson, C.T. Avedisian, J.C. Yang, *Int. J. Heat Mass Transfer* 35 (1992) 2017–2033.
[15] G.S. Jackson, C.T. Avedisian, *Proc. Roy. Soc. Lond. A* 446 (1994) 257–278.
[16] F.P. Incropera, D.P. DeWitt, T.L. Bergman, A.S. Lavine, *Introduction to Heat Transfer*, fifth ed., Wiley, New York, 2007.
[17] J.H. Bae, C.T. Avedisian, *Combust. Flame* 137 (2004) 148–162.
[18] B.J. Callahan, M.S. Thesis, Sibley School of Mechanical and Aerospace Engineering, Cornell University, 2000.
[19] C.T. Avedisian, G.S. Jackson, *J. Propul. Power* 16 (6) (2000) 974–979.
[20] G.J. Green, T.Y. Yan, *in: Proceedings of the 23rd Intersociety Energy Conversion and Engineering Conference*, ASME, New York, 1988, pp. 291–296.
[21] C.T. Avedisian, in: F.L. Dryer, R.F. Sawyer (Eds.), *Physical and Chemical Aspects of Combustion*, Gordon & Breach, Amsterdam, The Netherlands, 1997, pp. 135–160.
[22] R.A. Dobbins, *Combust. Flame* 130 (2002) 204–214.
[23] V. Nayagam, J.B. Haggard, R.O. Colantonio, et al., *AIAA J.* 36 (1998) 1369–1378.
[24] G.S. Jackson, C.T. Avedisian, *Int. J. Heat Mass Transfer* 41 (1998) 2503–2515.
[25] S.R. Turns, *An Introduction to Combustion*, second ed., McGraw-Hill, New York, 2000.
[26] W.A. Sirignano, *Fluid Dynamics and Transport of Droplets and Sprays*, Cambridge University Press, Cambridge, 1999, p. 17.
[27] B.D. Shaw, F.A. Williams, *Int. J. Heat Mass Transfer* 33 (1990) 301–317.
[28] S.H. Chung, C.K. Law, *Combust. Flame* 64 (1986) 237–241.
[29] B.H. Chao, C.K. Law, J.S. T'ien, *Proc. Combust. Inst.* 23 (1990) 523–531.
[30] A.J. Marchese, F.L. Dryer, R.O. Colantonio, *Proc. Combust. Inst.* 27 (1998) 2627–2634.
[31] S. Kumar, A. Ray, S.R. Kale, *Combust. Sci. Technol.* 174 (2002) 67–102.
[32] S.Y. Cho, M.Y. Choi, F.L. Dryer, *Proc. Combust. Inst.* 23 (1990) 1597–1604.
[33] G. Ben-dor, T. Elperin, B. Krasovitov, *Proc. Roy. Soc. Lond. A* 459 (2003) 677–703.